Am J Cancer Res 2026;16(1):105-124
www.ajcr.us /ISSN:2156-6976/ajcr0168313

Original Article

Matrine enhances RLS3-induced ferroptosis at non-toxic doses in acute myeloid leukemia cells with MLL rearrangement

Yaonan Hong[1,2*], Man Li[1,3*], Fanhua Yu[1,2,4*], Shiyue Wu[3], Shun He[1], Xiawan Yang[1,2,5], Peicheng Wang[1,2], Qi Liu[1,2], Yingying Shen[1,2,5], Guoyin Kai[3], Baodong Ye[1,2,5], Keding Shao[1,6], Dijiong Wu[1,2,5]

[1]Department of Hematology, The First Affiliated Hospital of Zhejiang Chinese Medical University (Zhejiang Provincial Hospital of Chinese Medicine), Shangcheng District, Hangzhou 310005, Zhejiang, P. R. China; [2]The First School of Clinical Medicine, Zhejiang Chinese Medical University, Binjiang District, Hangzhou 310053, Zhejiang, P. R. China; [3]Zhejiang Key TCM Laboratory for Chinese Resource Innovation and Transformation, Jinhua Academy, School of Pharmaceutical Sciences, Zhejiang Chinese Medical University, Binjiang District, Hangzhou 310053, Zhejiang, P. R. China; [4]Department of Internal Medicine, Shaoxing City Keqiao District Hospital of Traditional Chinese Medicine, Shaoxing 312000, Zhejiang, P. R. China; [5]National Traditional Chinese Medicine Clinical Research Base (Hematology), Shangcheng District, Hangzhou 310005, Zhejiang, P. R. China; [6]Office of Academic Research, Zhejiang Chinese Medical University, Binjiang District, Hangzhou 310053, Zhejiang, P. R. China. [*]Equal contributors.

Received August 24, 2025; Accepted January 4, 2026; Epub January 15, 2026; Published January 30, 2026

Abstract: Leukemia with MLL rearrangement (MLL-r) always exhibited a poor prognosis. Targeting ferroptosis was believed to be a novel strategy for the treatment of leukemia. However, the ferroptosis inducer, RSL3 (GPX4 inhibitor), was not clinically available due to its potential off-target effects and toxicity. This study aimed to explore whether the additional matrine (MAT) could yield superior therapeutic outcomes with ferroptosis inducer. Herein, we explored that MAT can synergistically induce ferroptosis with non-toxic dosage of RSL3 in MOLM-13 and MV4-11 cells. The underlying mechanism was investigated via western blot, quantitative RT-PCR (qRT-PCR) analysis, enzyme-linked immunosorbent assay (ELISA) and Flow cytometry. We found that the combination of MAT and non-toxic-dose RSL3 significantly increased levels of intracellular ferrous ion (IFI) and lipid ROS, decreased mitochondrial membrane potential and glutathione (GSH) levels, as well as down-regulated the expression of SLC7A11 and GPX4. Systematic bioinformatic analysis results have indicated that MAT may potentiate the efficacy of RSL3 through modulation of the p53 signaling pathway. Further experiments showed that knocking down p53 reduced the synergistic effect of MAT and RSL3 in inducing ferroptosis. In addition, the combination of MAT and RSL3 can dramatically reduce the population of bone marrow CD45+ cells in AML xenograft mouse. In conclusion, MAT can synergistically promote non-toxic-dose RSL3 induced ferroptosis by modulating the p53 pathway in AML with MLL translocation, which may potentially enable the clinical application of ferroptosis inducers in further.

Keywords: Matrine, MLL rearrangement, ferroptosis, leukemia, p53

Introduction

MLL rearrangement (MLL-r) is a frequent chromosomal anomaly in acute myeloid leukemia (AML), characterized by its high aggressiveness, low remission rates, recurrence likelihood, and shortened survival times [1]. Among AML cases, the MLL-AF9 fusion is particularly prevalent, accounting for approximately 30% of all MLL translocations [2, 3], while MLL-AF4 also attracted our attention due to its refractory nature. Most patients developed resistance and relapse during consolidation chemotherapy, resulting in a four-year overall survival rate of only approximately 29% [4, 5]. Therefore, the imperative to identify innovative therapeutic targets and develop groundbreaking interventions has become increasingly critical in addressing hematological malignancies. Ferroptosis, a distinct modality of regulated cell death characterized by iron-dependent lipid peroxidation, presents a compelling therapeu-

https://doi.org/10.62347/YKIG8290

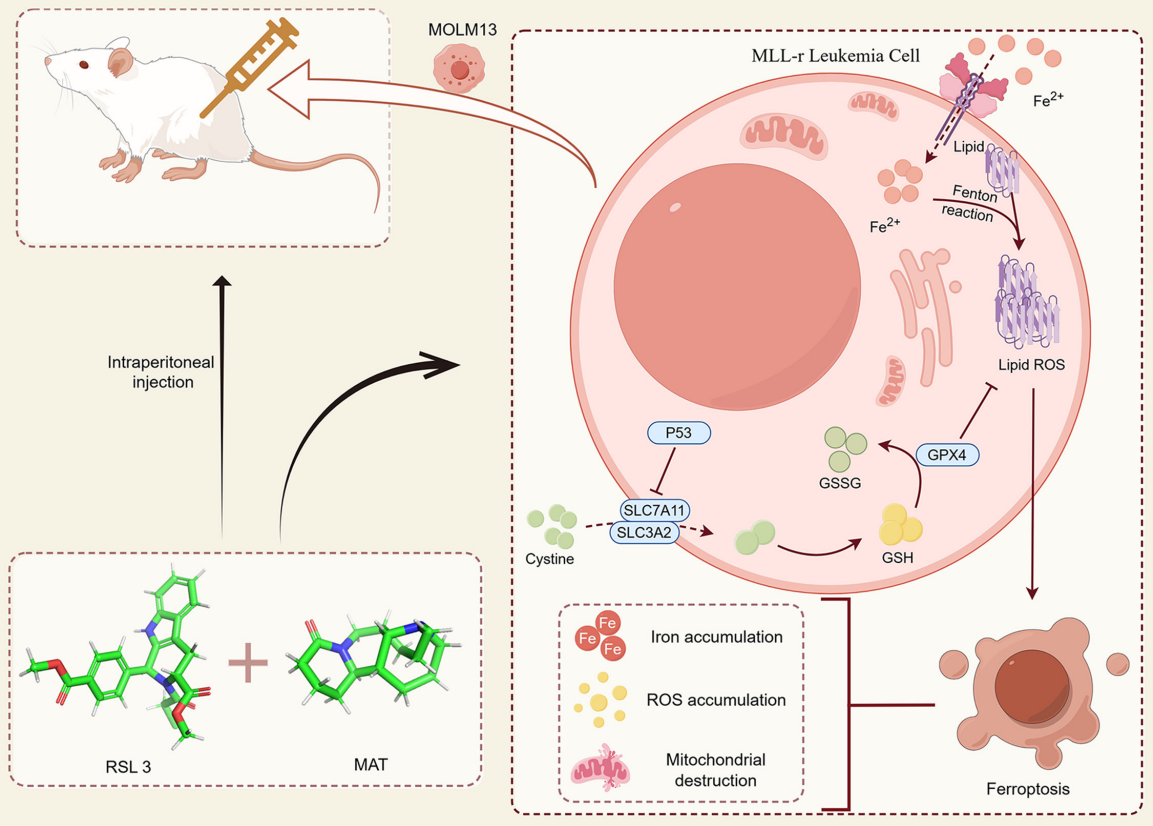

Figure 1. Graphical abstract.

tic strategy for leukemic cells. This is particularly relevant given their pathophysiological hallmark of aberrant intracellular iron accumulation, a phenomenon partially mediated by p53-dependent pathways [6, 7]. Ferroptosis activators like RSL3 may offer new therapeutic strategies for MLL-r leukemic cells by inducing ferroptosis [8]. Nevertheless, its clinical advancement and use were notably limited by its toxicity and adverse effects, such as liver and kidney dysfunction [9, 10].

Matrine (MAT), a quinoline alkaloid obtained from Sophora flavescens, shows a broad spectrum of pharmacological actions, including anti-inflammatory, immunosuppressive, and anti-tumor activities [11]. Current research has reported that the mechanisms of MAT in anti-leukemia are complex and diverse [12, 13], and there was a report indicating that MAT can against cervical cancer activity through the induction of ferroptosis [14]. Our team had earlier investigated the various possible impacts of MAT on treating blood cancers such as leukemia, lymphoma, and multiple myeloma, although the mechanisms were not completely explained [15-17]. This study demonstrates that while MAT alone does not trigger ferroptosis in AML, it can synergize with a non-toxic dose of RSL3 to enhance ferroptosis, potentially facilitating the clinical application of ferroptosis inducers (**Figure 1**).

Materials and methods

Cell culture

The MLL-r leukemic cell lines MOLM-13 (shCtrl, shp53) (CVCL number: 2119, MLL-AF9), MV4-11 (shCtrl, shp53) (CVCL number: 0064, MLL-AF4) cells were generously provided by Dr. Ya-Huei Kuo. The shRNA sequences used for the negative control (NC) and p53 knockdown are as follows: NC-TTCTCCGAACGTGTCACGT; p53-CGGCGCACAGAGGAAGAGAAT. These sequences are the target sequences used for each molecule. The human bone marrow stromal cell line HS-5 (CVCL number: 3720) was purchased from Cell Bank of Chinese Academy of Sciences (Shanghai, China). Cells were seed-

ed at an initial concentration of 1×10^5/ml in 1640 medium supplemented with 20% fetal bovine serum (FBS) and incubated 5% CO_2 at 37°C. Media were replaced every 48 h, and cells were observed and photographed to document their growth status.

Grouping

For *in vitro* study, cell lines (MOLM-13 and MV4-11) were grouped as follows: (1) control group (Ctrl), (2) MAT sole treated group (MAT), (3) RSL3 sole treated group (RSL3), (4) MAT and Fer-1 (Ferrostatin-1, a Ferroptosis inhibitor) co-treated group (MAT+Fer-1), (5) MAT and RSL3 co-treated group (MAT+RSL3), and (6) MAT, RSL3, and Fer-1 co-treated group (MAT + RSL3 + Fer-1).

Proliferation detection

Cells in the logarithmic growth phase were collected and seeded into a 96-well plate at 1×10^4 cell per well. Three replicate wells were set up for each sample. Following the addition of the corresponding concentrations of drugs, the cells were incubated in a constant-temperature incubator for 24, 48, and 72 h, respectively. 10 μL of CCK-8 solution (Shanghai Biosharp, QX1210) was added, and further incubated for 2 h. The absorbance was measured at 450 nm using a microplate reader, and the relative inhibition rate of the cells was calculated.

Apoptosis and necrosis detection

Leukemic cells in the logarithmic growth phase were collected, centrifuged, and counted. Cells were seeded into a 6-well plate at 1×10^5 cells per well. Cells were harvested after 48 hours of drug treatment, washed thrice with PBS, and resuspended in 500 μL of Binding Buffer. 5 μL Annexin V/FITC and 10 μL propidium iodide (PI) staining solution (Shanghai Yishan Biotechnology, AP001/100) were added and thoroughly mixed. Cells were kept in darkness at 37°C for 15 minutes. Apoptotic and necrotic rates were then analyzed using a flow cytometer. We have calibrated our flow cytometer regularly using beads with known fluorescence intensities to ensure accurate and consistent measurements. And we employed a rigorous gating strategy to identify and exclude cells with abnormal or non-specific staining patterns. This includes using forward and side scatter plots to gate on live, single cells and applying additional gates based on the staining patterns of specific markers to further refine our analysis (Supplementary Figure 1A).

Systematic bioinformatics analysis

The structural information of MAT was retrieved from the PubChem database. Potential targets of MAT were identified from Traditional Chinese Medicine Systems Pharmacology (TCMSP) and Search Tool for Interactions of Chemicals (STITCH), followed by the screening of AML-related targets using the GeneCards database. Subsequently, the UniProt database was employed to standardize and validate these targets. Venny was utilized to analyze the unique and shared components between MAT and AML groups. Search Tool for the Retrieval of Interacting Genes/Proteins (STRING) with Cytoscape was used to analyze these core targets. Cytoscape was also leveraged to construct a "compound-target-disease" network. Enrichment analyses of Kyoto Encyclopedia of Genes and Genomes (KEGG) and Gene Ontology (GO) for the core targets were conducted using R along with Bioconductor bioinformatics packages.

RNA-seq data from AML patient samples sourced from The Cancer Genome Atlas (TCGA) database and healthy donors from the Genotype-Tissue Expression (GTEx) database were analyzed using the stats and car packages in R. Visualization of the data was achieved using the ggplot2 package.

Molecular docking

Molecular docking between MAT and the core targets was performed using AutoDock Vina to validate their interaction activities. Pymol was utilized for visual analysis of the combinations with lower binding energies.

Intracellular ferrous ion (IFI) detection

Cells in the log phase were seeded into a 24-well plate. After 48 h of drug exposure, the cells underwent three washes with PBS. Then, 1 mL of a diluted FerroOrange fluorescent probe solution (DOJINDO, M489) was added, and incubated for 30 min in a cell culture incubator. Following this incubation, the 24-well plate was centrifuged at 1200 rpm for 5 min

Table 1. Primers for the target genes

Gene	Primer
GPX4	Forward: 5'-CCGCTGTGGAAGTGGATGAAGATC-3'
	Reverse: 5'-GCAGCCGTTCTTGTCGATGAGG-3'
SLC7A11	Forward: 5'-GGCTCCATGAACGGTGGTGTG-3'
	Reverse: 5'-GCTGGTAGAGGAGTGTGCTTGC-3'
GAPDH	Forward: 5'-TGTTGCCATCAATGACCCCTT-3'
	Reverse: 5'-CTCCACGACGTACTCAGCG-3'

and observed under a fluorescent inverted microscope for imaging. The image processing and fluorescence quantification for whole mount fluorescence were used ImageJ software.

Cellular lipid peroxidation detection

Cells in the log phase were seeded into a 6-well plate. Cells were harvested by centrifugation and rinsed with PBS after 48 hours of drug treatment. The cells were then resuspended in C11BODIPY581/591 lipid peroxidation fluorescent probe (GLPBIO, GC40165) at a final concentration of 5 μM and incubated in a 37°C incubator for 30 min. After incubation, cells were rinsed with PBS to eliminate surplus fluorescent probe. Lipid peroxidation levels in the cells were assessed via flow cytometry. Representative Fluorescence-Activated Cell Sorting (FACS) plots of lipid peroxidation is shown in Supplementary Figure 1B.

Mitochondrial membrane potential (Δψm) analysis

The JC-1 Mitochondrial Membrane Potential Assay Kit (Elabscience, E-CK-A301) was employed to assess mitochondrial membrane potential. Cells were exposed to the JC-1 staining solution in the dark at 37°C for 10 min. Subsequently, the cells underwent two washes with the working solution. Finally, the mitochondrial membrane potential was evaluated using a flow cytometer. Representative FACS plots of mitochondrial membrane potential is shown in Supplementary Figure 1C.

Glutathione (GSH) concentration detection

Cells in the log phase were seeded into a 6-well plate. After 48 hours of drug exposure, the supernatant was collected and stored in EP tubes for later analysis. GSH levels for each group were measured using the GSH ELISA Kit (Kelu Biotechnology, ELK7846) following the manufacturer's guidelines.

Quantitative real-time PCR (qRT-PCR) analysis

Reference to previous protocol in our laboratory for RNA extraction, reverse transcription, and qRT-PCR. GAPDH was used as a reference gene for its quantification [18]. The expression levels of GPX4 and SLC7A11 were quantitatively assessed. The $2^{-\Delta\Delta CT}$ method was employed to calculate differences in mRNA expression levels between groups. Refer to **Table 1** for the primer sequences.

Western blot (WB) analysis

Reference to previous protocol in our laboratory for WB analysis [18]. The membranes were incubated overnight with primary antibodies against SLC7A11 (Cell Signaling Technology (CST), #98051), GPX4 (CST, #52455), α-actinin (CST, #3134), p53 (CST, #2524), and β-actin (CST, #4970). Immunoreactive bands were visualized using anti-mouse and anti-rabbit secondary antibodies and an ECL chemiluminescent HRP substrate, followed by autoradiography. The band intensity was analyzed using ImageJ.

In vivo study

All animal protocols and procedures had approval from the Animal Experimental Research Center of Zhejiang Chinese Medicine University, Zhejiang, China (Ethics approval number: IACUC-20221121-02). The female NOD SCID gamma (NSG) mice, aged 5 weeks and obtained from Shanghai Nanfang Research Center in Shanghai, China. All mice were reared in clean animal laboratory of animal experimental research center of Zhejiang University of Chinese Medicine, with humidity 50%-70%, temperature 23-25°C, free feeding and drinking water, 12 h alternating light. NSG mice were randomly divided into five groups, each comprising nine mice: Vehicle group, MAT group (50 mg/kg), RSL3 group (5 mg/kg), MAT + RSL3 group (50 mg/kg MAT and 5 mg/kg), and Positive control group (50 mg/kg cytarabine (Ara-C) and 1.5 mg/kg daunorubicin

(DNR). Both RSL3 and MAT were administered via intraperitoneal injection every other day until euthanasia. For the positive control group (7+3 regimen), daunorubicin was injected via tail vein every other day for three doses, and cytarabine was injected intraperitoneally every other day for seven doses. 5×10^6 MOLM-13 cells transfected with luciferase were injected via the tail vein into NSG mice. *In vivo* imaging was performed once a week (day 7 and day 14), and fluorescence intensity, and tumor burden of the mice were observed after drug treatment. Body weights were measured every three days until they were euthanized. The specific criterion used to determine when animals should be euthanized is the onset of hind limb paralysis in the mice. Once this condition is observed, the mice are euthanized to prevent further suffering. Euthanasia was performed by administering pentobarbital sodium via intraperitoneal injection at a dose of 50 mg/kg to ensure the mice were fully anesthetized and free from pain. Following anesthesia, blood was collected via the abdominal aorta (0.5-1 mL). After blood collection, death was confirmed by observing the absence of respiration, heartbeat, corneal reflex, muscle tone, and mucosal color. Then, bone marrow was collected. Flow cytometry was employed to analyze the expression of CD45+ cells in the bone marrow of each group. Tissues from the heart, liver, spleen, lung, and kidney were gathered and weighed. Organ weight divided by body weight was used to compute organ indexes.

Serum was obtained from centrifuged blood to measure alanine aminotransferase (ALT), aspartate aminotransferase (AST), creatinine (CREA), and blood urea nitrogen (BUN) using a specific kit (Nanjing Jiancheng, China), following the manufacturer's instructions. Using an Auto Hematology Analyzer (Mindray Biomedical Electronics, Shenzhen, China), blood samples were obtained for regular blood index examination.

Statistical analysis

The *in vitro* studies were independently repeated in triplicate and the *in vivo* study used seven samples to confirm the findings. The experimental data were presented as mean ± standard deviation ($\bar{x} \pm S$) and analyzed using SPSS 23.0 software. Analysis of Variance (ANOVA) was chosen for data analysis after confirming the normality of the data (Shapiro-Wilk test) and equality of variances (Levene's test). Post hoc comparisons were performed using Tukey's HSD test to ensure robust and accurate multiple group comparisons while controlling for Type I error. A *P*-value of less than 0.05 was considered statistically significant. Graphical representations of the results were generated using GraphPad Prism 8 software.

Results

MAT synergizes with ferroptosis inducer RSL3 to exert anti leukemia effect in MLL-r AML cell lines

The inhibitory effect of MAT on MOLM-13 (MLL-AF9) and MV4-11 (MLL-AF4) cells proliferation was evaluated. The results reveal that the inhibitory effect of MAT on MLL-r cell lines correlated positively with both its concentration and treatment duration (**Figure 2A-C**). The experiment was used to determine the concentration required to induce the desired biological effect without causing significant cytotoxicity. But this effect could not be reversed by the ferroptosis inhibitor Fer-1 (**Figure 2D**). Meanwhile, RSL3 alone demonstrated a concentration-dependent inhibitory effect (**Figure 2E**). Combining the two drugs yielded a significant synergistic index, measuring 15.711 and 17.931 in MOLM-13 and MV4-11 cells, respectively (**Figure 2F**, **2G**). This synergy was completely reversed by Fer-1 (from 26.42% to 72.01%) (**Figure 2H**). And Fer-1 did not affect the cell viability of MOLM-13 and MV4-11 (Supplementary Figure 2A, 2B). Further experiments revealed potent synergistic cytotoxicity even at non-toxic and low doses of both drugs. In addition, we explored the effects of combining MAT with another ferroptosis inducers, Erastin. The results indicated that MAT is less effective in inducing ferroptosis in MOLM-13 cells when combined with Erastin compared to RSL3, with a synergistic index of 9.63 (Supplementary Figure 3). Consequently, we selected 1 μM RSL3 (resulting in 96.17% cell viability) and 1 mM MAT for MOLM-13 cells, and 0.125 μM RSL3 (resulting in 95.03% cell viability) and 0.25 mM MAT for MV4-11 cells for subsequent exploration. The combination exhibited significant effects in MOLM-13 and MV4-11 cells, with necrosis rates (PI+) for the Ctrl, MAT,

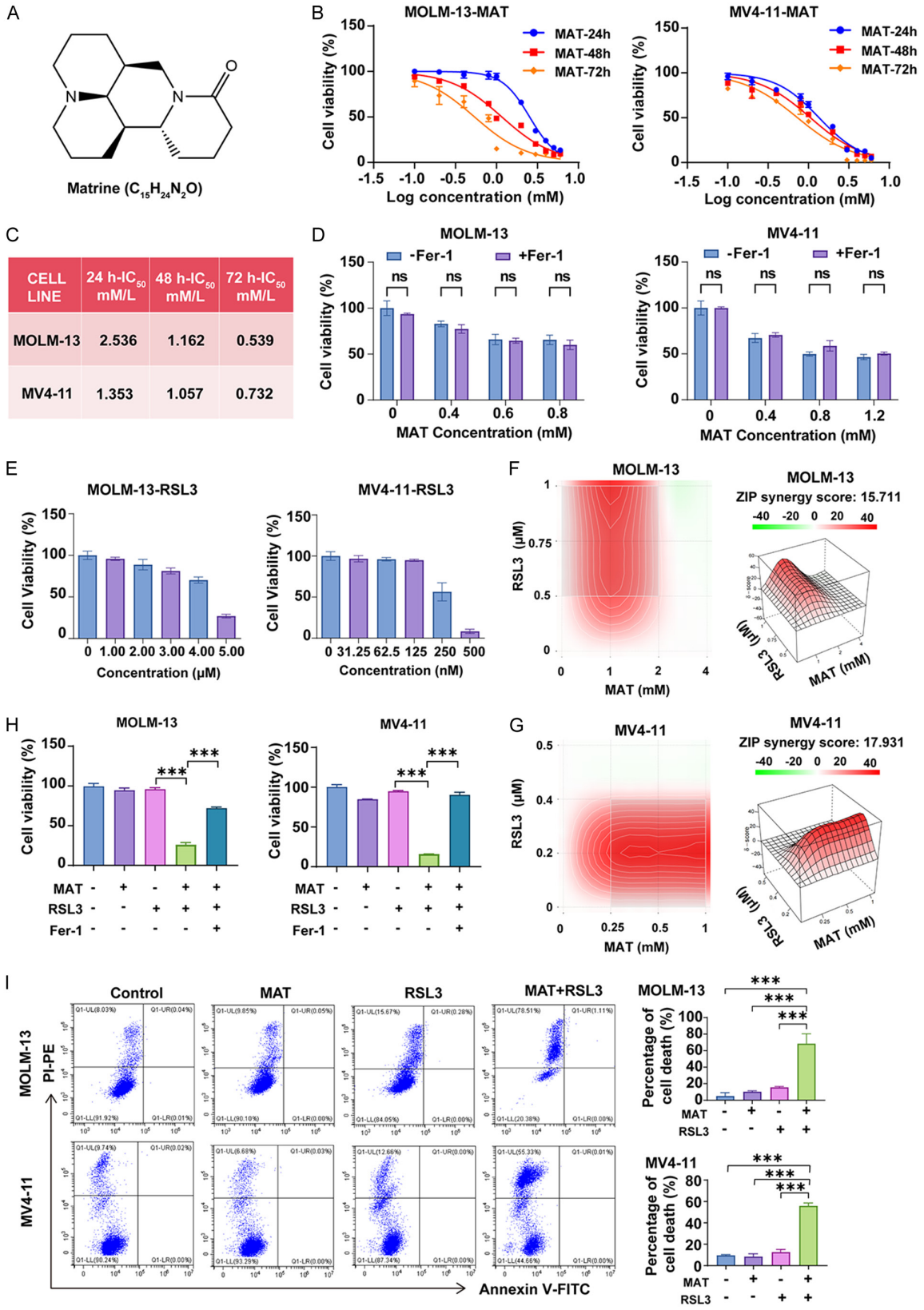

Figure 2. The synergistic effect of matrine and RSL3 on inducing MLL rearrangement (MLL-r) leukemic cell death. A. Molecular structural formula of matrine. B. Analysis of cell viability. Different concentrations of matrine were used to act on MOLM-13 and MV4-11 cell lines for different durations. C. Quantification of IC_{50} values of matrine in MOLM-

CELL LINE	24 h-IC_{50} mM/L	48 h-IC_{50} mM/L	72 h-IC_{50} mM/L
MOLM-13	2.536	1.162	0.539
MV4-11	1.353	1.057	0.732

13 and MV4-11 cell lines. D. Incubation of the ferroptosis inhibitor Fer-1 with matrine in MOLM-13 and MV4-11 cells for 48 h. E. Use of different concentrations of RSL3 to act on MLL-AF9 leukemia cells. F, G. Synergy score of matrine combined with RSL3 in the treatment of MOLM-13 and MV4-11 cells. H. Reversal of cell death caused by matrine combined with RSL3 by the ferroptosis inhibitor Fer-1. I. Determination of the rate of necrotic cells by flow cytometry. Data were represented as mean ± SD, n = 3. ***$P < 0.001$.

RSL3, and MAT + RSL3 groups being 8.07%, 9.90%, 15.95%, and 79.62% in MOLM-13 cells, and 9.76%, 6.71%, 12.66%, and 55.34% in MV4-11 cells, respectively (**Figure 2I**). Meanwhile, the inhibition rate of RSL3 on bone marrow stromal cell line, HS-5, was lower than in MOLM-13 and MV4-11 cells, and MAT (1 mM) did not enhance the inhibitory effect of RSL3 on HS-5 cell proliferation (Supplementary Figure 4), suggesting that the combination of MAT and RSL3 has a favorable safety profile.

MAT sensitize cells to ferroptosis

Our previous findings indicated that the combination of MAT and RSL3 resulted in substantial cell death, the specific form of which remained unclear. Given RSL3's properties, ferroptosis was considered highly plausible. Initially, we assessed changes in IFI levels. The findings indicated that IFI levels did not increase with either MAT or RSL3 treatment alone. The combined treatment of MAT and RSL3 significantly increased IFI accumulation in both cell lines ($P < 0.01$) (**Figure 3A**), accompanied by up-regulated expression of intracellular lipid peroxidation ($P < 0.05$) (**Figure 3B**). Additionally, the synergistic regimen induced significant reductions in both mitochondrial membrane potential (**Figure 3C**) and GSH levels (**Figure 3D**, **3E**) compared to monotherapy ($P < 0.05$). To validate the combined impact on ferroptosis pathway regulation, we evaluated the expression levels of proteins associated with ferroptosis. The results showed that MAT + RSL3 could down-regulate the expression of SLC7A11 protein in MOLM-13 cells, but had no effect on GPX4 expression. Notably, MAT + RSL3 significantly reduced the expression of both GPX4 and SLC7A11 proteins in MV4-11 cells (**Figure 3F**, **3G**).

Systematic bioinformatic analysis of MAT treatment for AML

To explore how MAT promotes ferroptosis, bioinformatics analysis will be used to investigate the primary mechanism of action. We comprehensively collected data on 20 potential targets of MAT and 8,309 AML-associated targets. Ultimately, 16 targets were identified as crucial for both MAT and AML (**Figure 4A**). Subsequently, we analyzed the PPI network among these overlapping targets and ranked them based on their Degree values (**Figure 4B**, **4C**). Potential targets include PTEN, CASP3, and CCND1, etc. GO enrichment analysis yielded a total of 1,130 results. The Biological Processes (BP) mainly involved responses to UV, regulation of apoptotic signaling pathways, and leukocyte cell-cell adhesion. The Cellular Components (CC) mainly involved membrane rafts, membrane microdomains, and transcription repressor complexes. The Molecular Functions (MF) mainly involved protease binding, ATP-dependent chromatin remodeler activity, and core promoter sequence-specific DNA binding (**Figure 4D**). The KEGG enrichment analysis identified 103 enriched pathways, primarily involving the AGE-RAGE signaling pathway in diabetic complications, Epstein-Barr virus infection, and Proteoglycans in cancer, etc. (**Figure 4E**). Notably, our findings suggest that MAT may exert its therapeutic effects on AML through the acute myeloid leukemia and p53 signaling pathways, with key molecules such as RELA, CASP3, MYC, PTEN, and CCND1 playing pivotal roles (**Figure 4F-H**). Furthermore, we observed significant differences in the expression levels of p53, RELA, CASP3, MYC, PTEN, and CCND1 between RNA-seq data derived from AML patients and healthy donors (**Figure 4I**).

Molecular docking

Investigating the affinity between potential molecules and proteins is crucial for identifying targets. A lower binding energy in molecular docking indicates a tighter interaction between the receptor and ligand, suggesting a stronger binding capacity. Our research revealed that MAT exhibited binding energies ≤ -5.0 kcal·mol^{-1} with p53, RELA, CASP3, MYC, PTEN, and CCND1, indicating good binding affinity (**Figure 5A-F**; **Table 2**). These data collectively suggest that MAT may play a significant role in anti-AML activity through the p53-mediated downstream

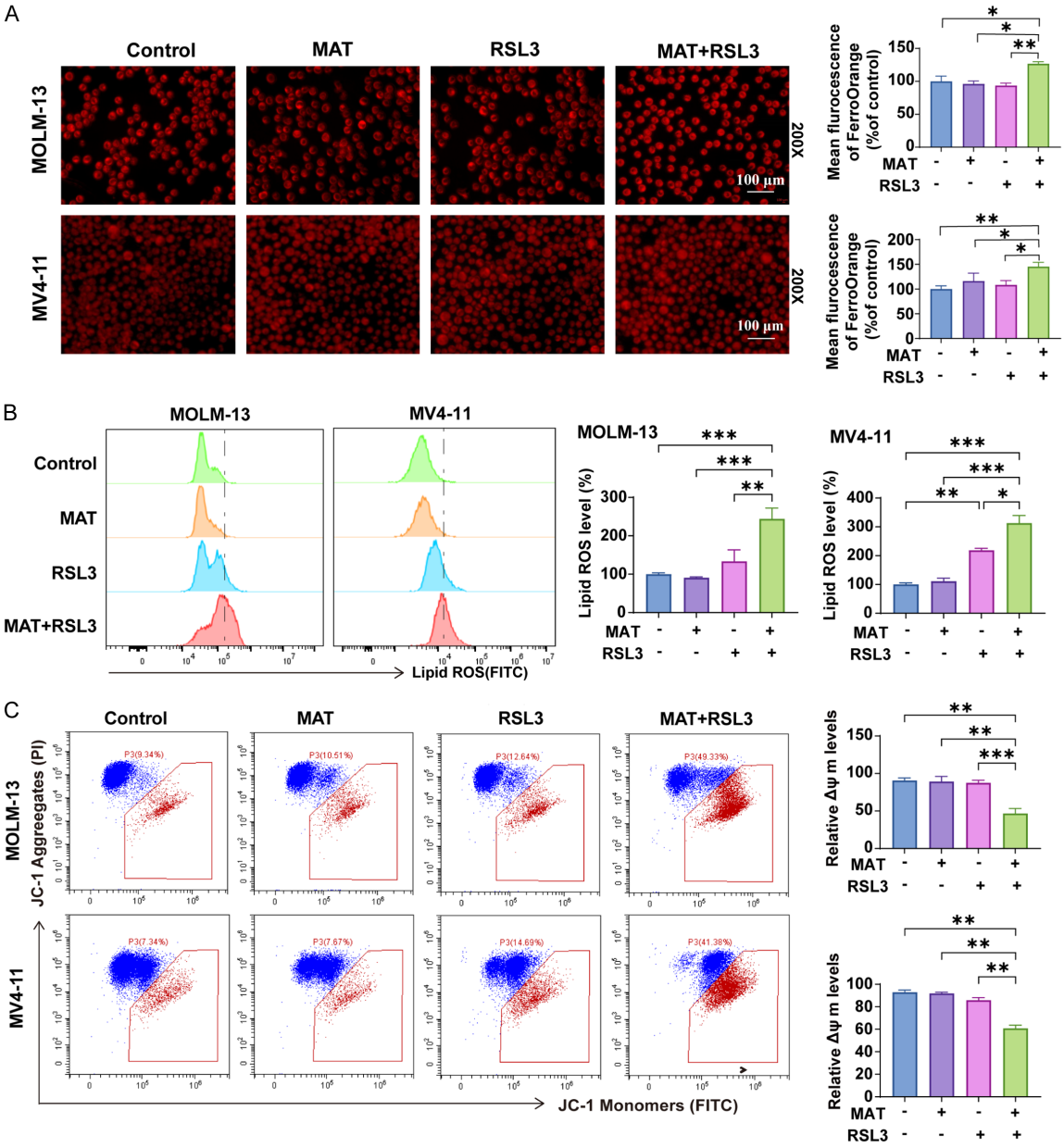
A
Control
MAT
RSL3
MAT+RSL3
MOLM-13
MV4-11
200X
100 μm
Mean flurocescence of FerroOrange (%of control)
MAT
RSL3
B
MOLM-13
MV4-11
Control
MAT
RSL3
MAT+RSL3
Lipid ROS(FITC)
Lipid ROS level (%)
C
JC-1 Aggregates (PI)
JC-1 Monomers (FITC)
Relative Δψ m levels
D
MOLM-13 GSH(ng/mL)
E
MV4-11 GSH(ng/mL)
F
G
SLC7A11
GPX4
α-Actinin
Relative expression
Ctrl
Matrine
RSL3
Matrine+RSL3

Figure 3. Matrine potentiates the ferroptosis induced by RSL3 in leukemia cells. A. Measurement of intracellular ferrous ion levels in each group. B. Flow cytometry analysis of lipid peroxidation ROS. C. Flow cytometry analysis of mitochondrial membrane potential. D, E. Elisa analysis of serum glutathione (GSH) levels. F, G. Analysis of the expression of GPX4 and SLC7A11 in MLL-AF9 leukemic cell line by western blotting, with α-actinin used as the reference control. Data were represented as mean ± SD, n = 3. *$P < 0.05$, **$P < 0.01$, ***$P < 0.001$.

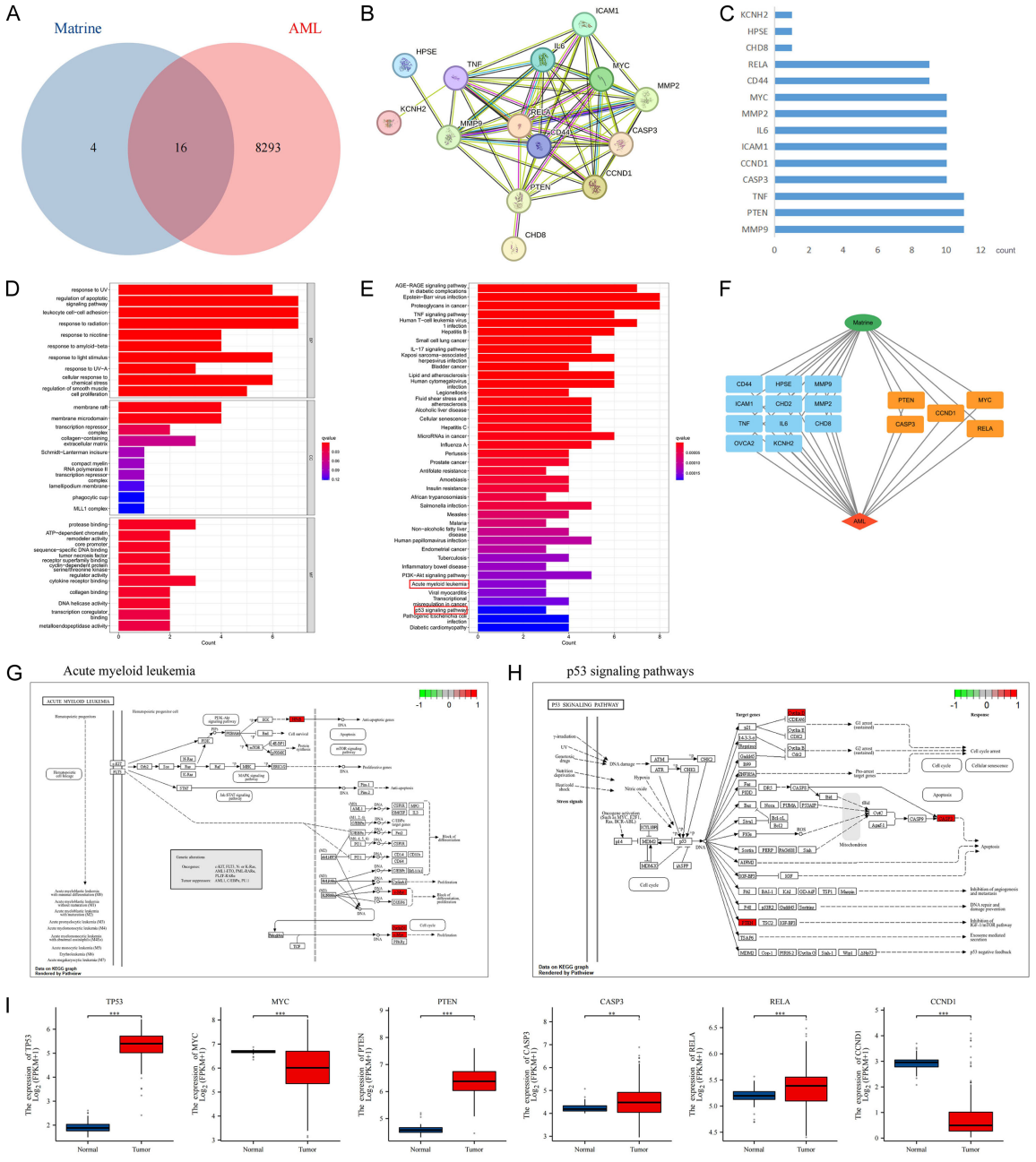

Figure 4. Key pathways for the MAT treatment of AML. A. The Venn plot of MAT and AML. B. PPI network of targets. C. Screened AML targets of MAT. D. GO analysis. E. KEGG analysis. F. "compound-target-disease" network. G. acute myeloid leukemia. H. p53 signaling pathways. I. Differential expression of key molecules in AML patients and healthy donors.

pathways. Furthermore, given RSL3's properties, we considered that MAT combined with RSL3 to treat AML may have a significant correlation with mediating p53 protein and activating of the downstream ferroptosis pathway.

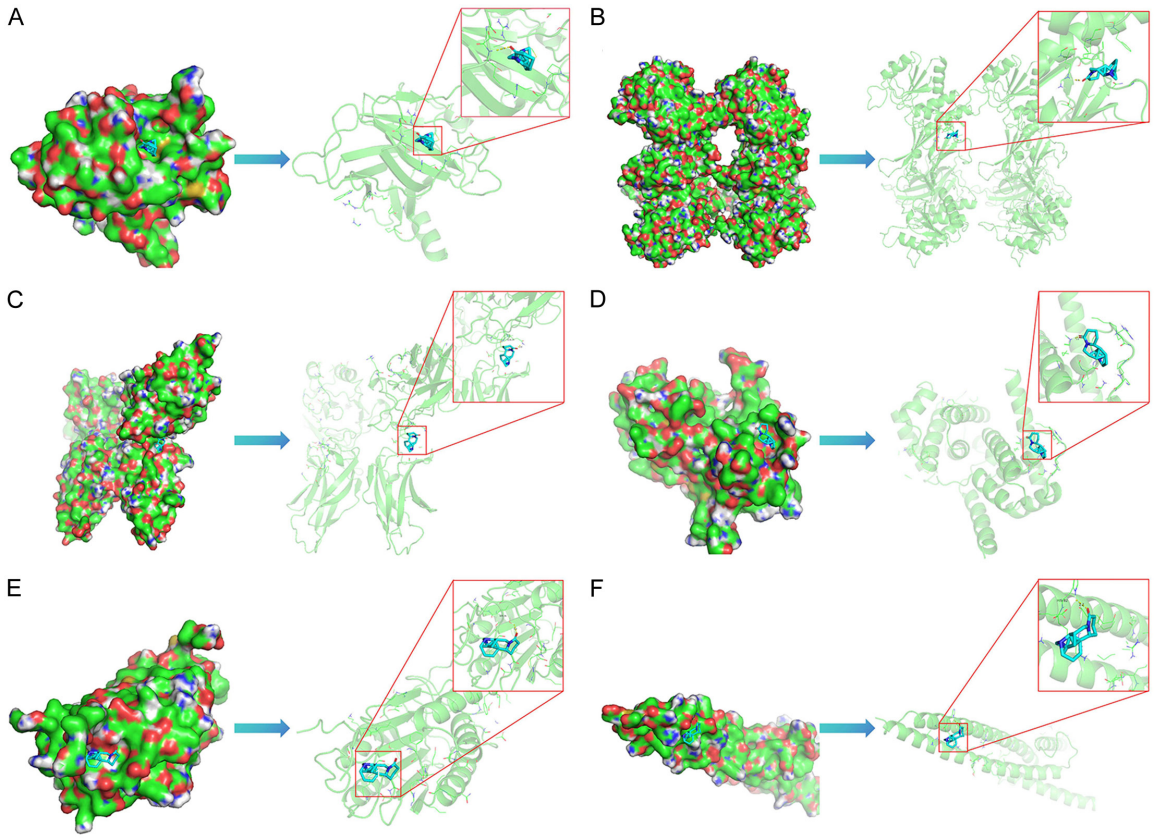

Figure 5. Results of molecular docking between Matrine and typical targets. A. p53 - Matrine. B. PTEN - Matrine. C. RELA - Matrine. D. CCDN1 - Matrine. E. CASP3 - Matrine. F. MYC - Matrine.

Table 2. Details of molecular docking between matrine and typical targets

Targets	Gene name	PDB number	Energy of binding (kcal • mol-1)	Number of bonds	Binding site	Length of bond (Å)
Tumor protein p53	TP53	1kzy	-5.7	1	LEU-264	2.5
RELA proto-oncogene	RELA	9bdv	-6.1	1	GLN-29	2.0
Caspase 3	CASP3	2cjx	-6.5	1	SER-36	2.2
MYC proto-oncogene	MYC	5i50	-5.0	1	HIS-82	2.2
Phosphatase and tensin homolog	PTEN	5bug	-7.7	1	ARG-173	2.0
Cyclin D1	CCND1	6p8e	-6.8	1	HIS-181	2.0

MAT promotes ferroptosis in MLL-r cells via p53/SLC7A11/GPX4 pathway regulation

The knockdown efficiency of p53 in MOLM-13 and MV4-11 cells was repeatedly confirmed by WB analysis (**Figure 6A**). In MOLM-13 shp53 and MV4-11 shp53 cells, the synergy coefficients of the two drugs were 7.756 and 10.98, respectively (**Figure 6B**, **6C**). We observed that MAT + RSL3 had no significant effect on p53 protein levels, although the knockdown of p53 reduced the combined effect in the two cell lines. In MOLM-13 shCtrl cells, necrosis rates were 10.79% for Ctrl, 15.58% for MAT, 16.94% for RSL3, and 82.39% for MAT + RSL3 groups. In MV4-11 shCtrl cells, the rates were 11.71% for Ctrl, 7.61% for MAT, 16.44% for RSL3, and 54.85% for MAT + RSL3 groups. In MOLM-13 shp53 cells, the rates were 3.70%, 2.03%, 3.27%, and 2.95%, while in MV4-11 shp53 cells, they were 5.92%, 10.22%, 6.62%, and 16.53% (**Figure 6D**). Moreover, MAT combined with RSL3 significantly enhanced intracellular lipid peroxidation expression in shCtrl cell lines

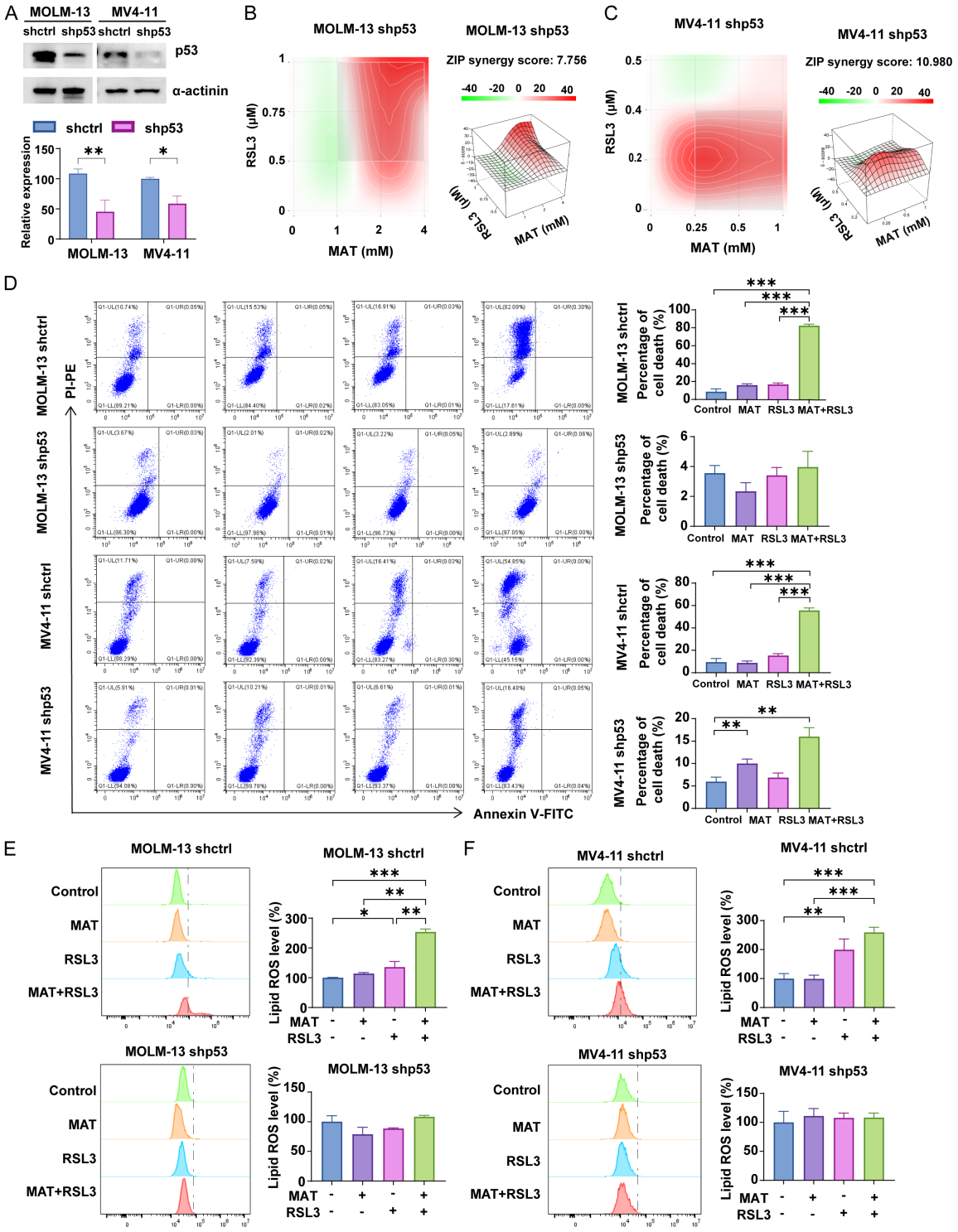

Figure 6. The role of p53 in the synergistic induction of ferroptosis by matrine and RSL3. A. The effect of p53 knockdown on protein levels of p53 in MOLM-13 and MV4-11 cells was determined using western blotting, with β-actin as the reference control. B, C. Synergy score of matrine combined with RSL3 in the treatment of MOLM-13 shp53 and MV4-11 shp53 cells. D. Determination of the rate of necrotic cells. E, F. Measurement of the level of lipid peroxidation ROS by flow cytometry. Data were represented as mean ± SD, n = 3. *$P < 0.05$, **$P < 0.01$, ***$P < 0.001$.

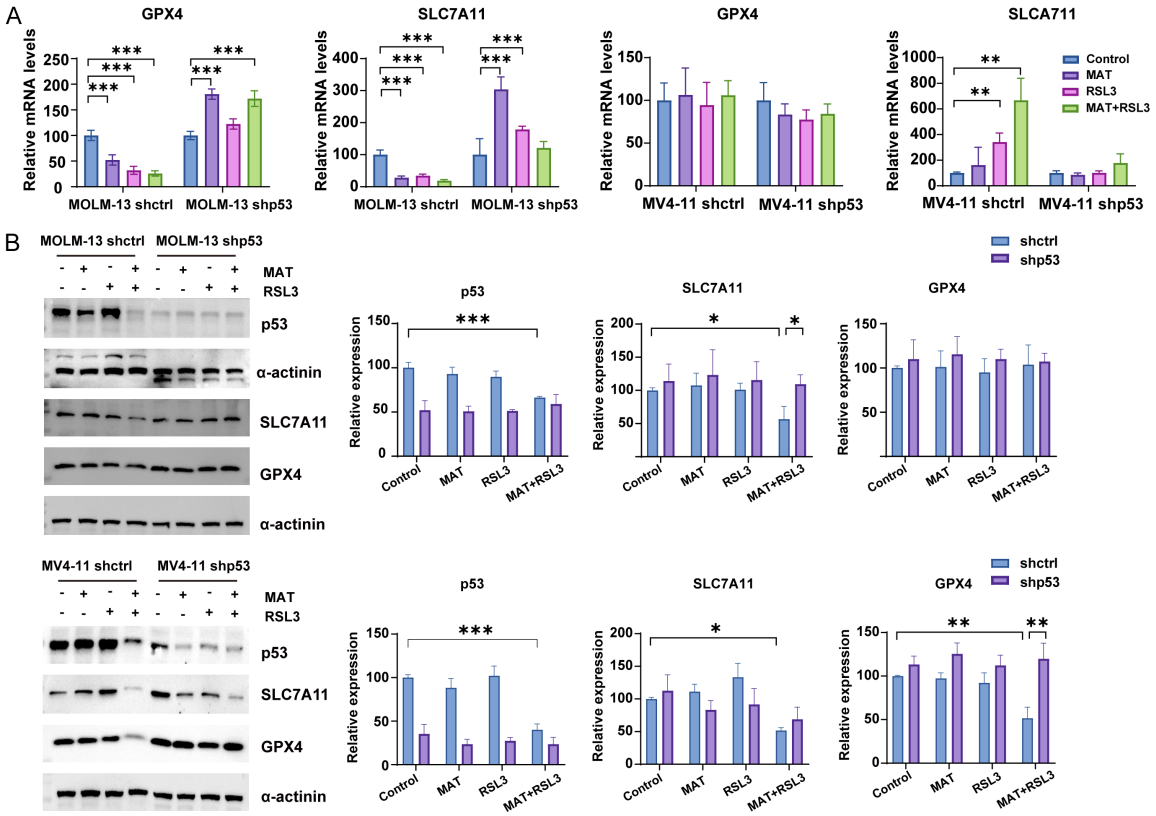

Figure 7. The impact of matrine on the ferroptosis pathway in MLL-r leukemia cells. A. Analysis of GPX4 and SLC7A11 gene expression in MLL-AF9 leukemic cell lines using qRT-PCR. B. Protein levels of p53, GPX4, and SLC7A11 in MLL-AF9 leukemic cell lines were analyzed by western blotting, with α-actinin used as the reference control. Data were represented as mean ± SD, n = 3. **P* < 0.05, ***P* < 0.01, ****P* < 0.001.

(*P* < 0.05). Lipid peroxidation levels in both shp53 cell lines did not significantly differ from the Ctrl group (**Figure 6E**, **6F**). Treatment with MAT+RSL3 significantly downregulated both mRNA and protein levels of p53 and SLC7A11 in MOLM-13 cells, whereas p53 knockdown reversed these effects. In MV4-11 cells, MAT+RSL3 upregulated SLC7A11 mRNA expression but reduced p53, GPX4 and SLC7A11 protein levels, with p53 knockdown partially restoring GPX4 protein expression. These findings demonstrate cell type-dependent differential regulation of ferroptosis-related molecules by MAT+RSL3 through p53-mediated mechanisms (**Figure 7A**, **7B**).

The combined treatment of MAT and RSL3 significantly suppresses tumor progression in AML xenograft mouse models

In vivo imaging revealed that mice treated with both MAT and RSL3 exhibited reduced fluorescence intensity by day 14 compared to the Vehicle group, while no significant changes were noted in groups treated with only MAT or RSL3 (**Figure 8A**). The bone marrow's CD45+ cell proportion significantly decreased in the RSL3, MAT + RSL3, and Ara-c + (Positive control) groups (*P* < 0.05), with the Positive control group showing the lowest proportion at 10% (**Figure 8B**, **8C**). Mouse weight did not differ significantly between groups throughout the treatment period (**Figure 8D**). Meanwhile, MAT had little effect on the indexes of heart, liver, spleen, lung and kidney, as well as serum AST, ALT, CREA, and CREA levels. Our hematological results revealed that platelet counts in the MAT + RSL3 group (332.42 × 10^9/L) were slightly elevated compared to the model group (296.5 × 10^9/L), while the standard AML chemotherapy group (7 + 3 regimen) showed a significant increase in platelet counts (649.14 × 10^9/L, *P* < 0.05). Existing literature has reported that high platelet counts are associated with poorer treatment outcomes and shorter relapse-free survival in AML patients, particularly in interme-

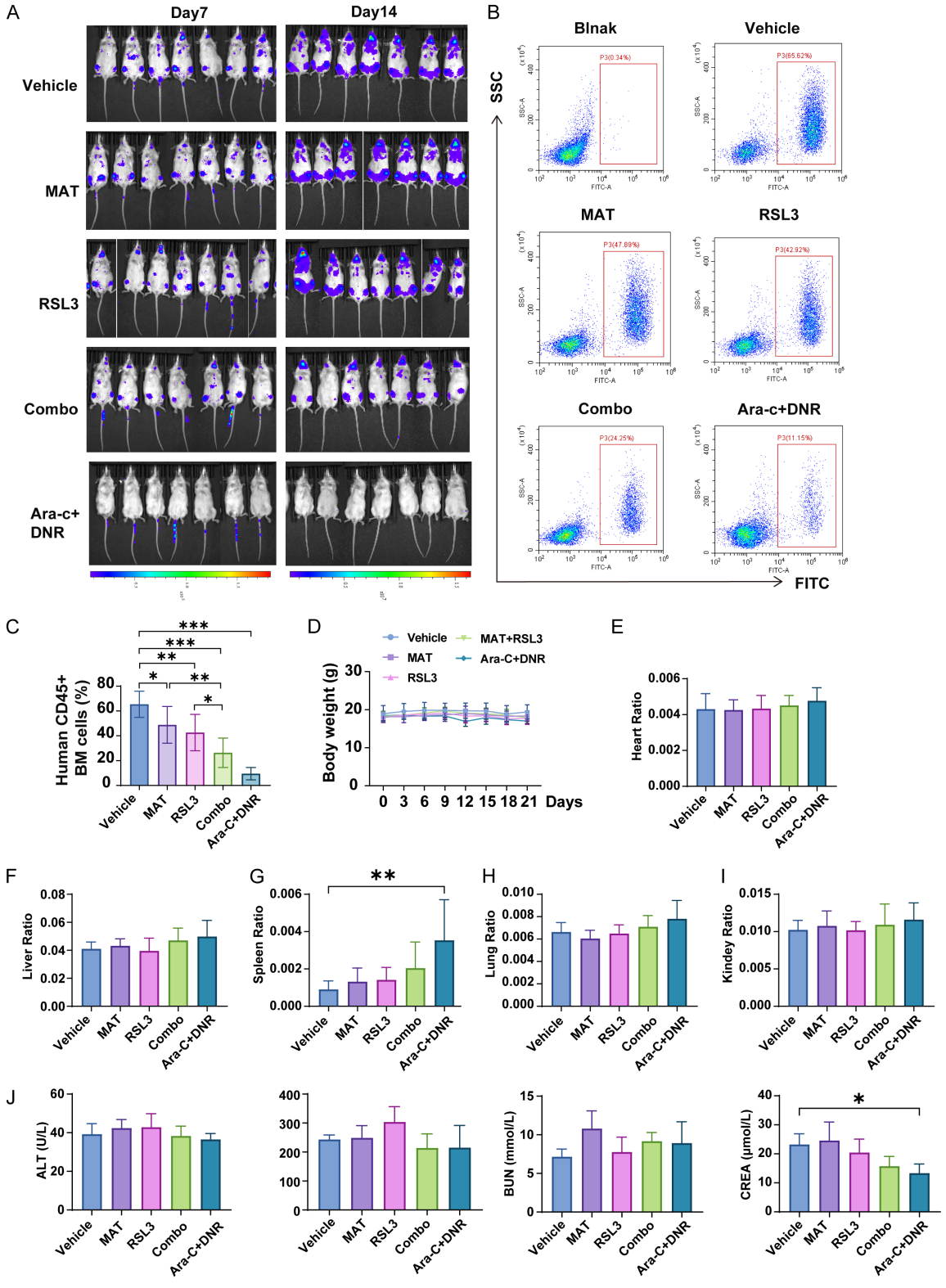

Figure 8. Anti-leukemia efficacy of matrine combined with RSL3 *in vivo*. A. Bioluminescent images of mice post therapy on Days 7 and 14. B, C. Flow cytometry analysis of the expression of CD45+ cells in the bone marrow. D. Every three days, mice's bodyweight was measured during therapy. E-I. Effect of matrine combined with RSL3 on organ indexes. J. Effect of matrine combined with RSL3 on serum biochemical levels alanine aminotransferase (ALT), aspartate aminotransferase (AST), creatinine (CREA), and blood urea nitrogen (BUN). Data were represented as mean ± SD, n = 7. $*P < 0.05$, $**P < 0.01$, $***P < 0.001$.

diate-risk AML [19]. Other hematological parameters showed no significant differences between the standard chemotherapy group and the MAT + RSL3 group. The spleen, as an important immune organ, serves as a critical indicator for assessing drug-induced immunotoxicity through its mass and histopathological changes. Our findings demonstrated that the spleen index in the standard chemotherapy group was significantly increased compared to the model group, suggesting potential physiological or pathological changes in the spleen. In contrast, MAT + RSL3 treatment did not significantly alter the spleen index, indicating a more favorable safety profile (**Figure 8E-J**). Additionally, blood routine indices were unaffected by MAT. RSL3, alone or combination (Supplementary Table 1). These results indicate that mat+rsl3 has better safety compared with Ara-c +DNR.

Discussions

Ferroptosis, a widespread cellular death mechanism found in various organisms, has been closely linked to tumorigenesis, especially in highly metastatic cancer cells (e.g., leukemia) [20, 21]. Researchers have been investigating novel approaches utilizing ferroptosis to improve the prognosis of AML patients [22, 23]. However, the adverse effects of ferroptosis activators have significantly impeded their clinical application [9, 10, 24]. Thus, devising strategies to achieve superior therapeutic outcomes with lower doses of RSL3 is essential. As a quinolizidine alkaloid, MAT exhibits moderate oral bioavailability, relatively stable plasma concentration levels, and significant anti-inflammatory, antiviral, and analgesic effects [25]. Furthermore, it demonstrates anticancer potential by inducing ferroptosis [14]. Comprehensive pharmacokinetic studies, especially regarding leukemia treatment and combination therapies, are essential to evaluate its clinical applicability. This study aims to enhance understanding of the biological role of ferroptosis in MLL-r leukemia and to identify potential new therapeutic targets and drugs for leukemia.

Our study found that combining non-toxic doses of RSL3 and MAT synergistically increased cytotoxicity in MOLM-13 and MV4-11 cells, an effect reversible by the ferroptosis inhibitor Fer-1, chosen for its proven specificity and efficacy. This approach allowed us to directly compare the effects of inhibiting ferroptosis to those observed in its absence, providing clearer insights into the mechanism underlying our observations. Our results revealed that MV4-11 and MOLM-13 exhibit different sensitivities to RSL3, which may be attributed to differences in their genetic backgrounds. The incubation times for cytotoxicity assays were chosen based on preliminary experiments and literature precedence [26], as they effectively capture the dynamic range of ferroptosis induction, allowing observation of its initiation, progression, and outcomes in cell viability, ensuring a comprehensive evaluation aligned with established experimental frameworks. Furthermore, we have also evaluated the synergistic effects of MAT with another ferroptosis inducer, Erastin, and found that the combination index of MAT + Erastin (9.63) was lower than that of MAT + RSL3 (15.711). This difference may be related to the target specificity of different ferroptosis inducers. In future studies, we plan to evaluate the synergy index of MAT in combination with various ferroptosis inducers to further explore its role in sensitizing ferroptosis and to identify potential common targets. To identify the most effective drug combinations, we plan to use ZIP synergy scoring or high-throughput screening to evaluate existing ferroptosis inducers and standard chemotherapeutic agents in combination with MAT. This approach will help us identify the optimal synergistic partners for MAT and further explore its therapeutic potential.

While our data suggest that the cell death induced by the combination of MAT and RSL3 is primarily mediated through ferroptosis, as demonstrated by the reversal of effects with the ferroptosis inhibitor Fer-1, potential off-target effects of MAT or RSL3 cannot be entirely ruled out. Future studies should explore these possibilities through more extensive pharmacological and genetic approaches, such as genetic manipulation of ferroptosis regulators and high-throughput screening, to confirm the specificity of ferroptosis induction and identify any confounding off-target interactions.

Ferroptosis as a novel iron-dependent form of cell death is different from other traditional cell death methods, characterized by abnormal

increase of IFI and lipid ROS [27, 28]. The redox state of GSH is crucial in regulating ferroptosis, which can be triggered by its depletion [29]. Upon the onset of ferroptosis, mitochondria exhibit atrophy characterized by increased membrane density, diminished or absent cristae, degeneration, and a notable reduction or loss of membrane potential [30]. Our study demonstrated that administering the two drugs simultaneously led to increased levels of lipid ROS and IFI and decreased levels of mitochondrial membrane potential and GSH compared to monotherapy. These findings demonstrated that MAT promotes ferroptosis when combined with non-toxic doses of RSL3. Furthermore, An AML xenograft mice model was utilized to validate the synergistic effect of MAT and RSL3. The xenograft model of AML has demonstrated considerable potential in mimicking key aspects of the disease, including leukemic cell infiltration into the bone marrow, spleen, and peripheral blood, as well as genetic and molecular heterogeneity. While the model cannot fully replicate the complexity of human AML, it has proven valuable for studying disease progression and therapeutic responses, providing insights that often correlate with clinical outcomes. In our study, we chose female NSG mice for the AML model because they are generally more docile, which facilitates long-term experimental management. Additionally, this choice avoids the potential influence of male hormones (e.g., testosterone), which may promote inflammatory responses or certain tumor progression [31, 32]. The combination treatment of MAT and RSL3 in mice resulted in reduced fluorescence intensity and a decreased percentage of CD45+ cells in the bone marrow. The findings indicate that employing MAT to enhance the sensitivity of ferroptosis may reduce treatment duration and enhance therapeutic efficacy. Future studies will aim to address potential sex-specific differences by including both male and female cohorts.

The SLC7A11/GPX4 pathway is a well-established signaling mechanism in ferroptosis. Under normal conditions, this pathway protects cells from ferroptosis by maintaining low levels of lipid peroxidation. However, when the function of GPX4 is compromised, either through genetic mutation, pharmacological inhibition, or depletion of its substrate GSH, cells become susceptible to ferroptosis. In our study, we observed that the combination of MAT and RSL3 can downregulate the expression level of SLC7A11 and GPX4, as well as lipid peroxidation levels and necrosis rate in MOLM-13 and MV4-11 cells, but the underlying mechanism is unclear. Network pharmacology is an important tool for investigating drug mechanisms of action and elucidating the pathological networks of complex diseases [33]. Systematic pharmacological studies suggest that MAT may exert its therapeutic effects on AML through the p53 signaling pathway, supported by molecular docking results showing MAT's strong binding affinity with key proteins of this pathway, including p53, RELA, CASP3, MYC, PTEN, and CCND1. These molecules are interconnected in the regulation of ferroptosis, and the observed synergistic effect of MAT and RSL3 in inducing ferroptosis is likely mediated through the complex interplay of these pathways. While MAT may potentially influence other regulatory pathways, our findings suggest that its effects on ferroptosis are particularly mediated through p53, making this interaction a key focus of our study. And future studies should include co-immunoprecipitation or other relevant experimental techniques to validate these predicted interactions and to provide more concrete evidence supporting the role of MAT in modulating the p53 signaling pathway and its downstream effects in AML. P53, a crucial tumor suppressor, primarily exerts its anti-leukemic effects through cell cycle arrest, induction of differentiation, and promotion of apoptosis and autophagy [34]. Many studies have proved that the activation of p53 is significantly correlated with the occurrence of ferroptosis [6, 35, 36]. It is reported that p53 can disrupt the cystine-glutamate antiporter system Xc- by inhibiting SLC7A11 expression, reducing cystine uptake, and promoting the activation of the ROS system, thereby leading to the occurrence of ferroptosis in tumor cells [37]. Consistently, knocking down p53 can ameliorate the ferroptosis in AML cells. MAT+RSL3 downregulated SLC7A11 and p53 in MOLM-13 and MV4-11 cells. This suggests that the induction of ferroptosis in leukemic cells by the combination of MAT and RSL3 is regulated by p53. Notably, we found that MAT+RSL3 significantly inhibited the expression of GPX4 in MV4-11, but not in MOLM-13. The observed discrepancy in GPX4 expression levels between the two cell lines likely arises from their distinct

susceptibility to ferroptosis. The concentration of MAT+RSL3 inducing ferroptosis in MLL-r cells was several times different (1 μM *VS.* 0.125 μM in RSL3 and 1 mM *VS.* 0.25 mM in MAT). In MV4-11 cells, MAT+RSL3 not only inhibited the function of GPX4, but also reduced its expression, which may be the reason why MV4-11 is more sensitive to ferroptosis. On the other hand, although GPX4 is a key regulator of the ferroptosis pathway, its activity is influenced not only by protein expression levels but also by multiple regulatory mechanisms. First, the activity of GPX4 can be altered by post-translational modifications (such as ubiquitination and phosphorylation), which in turn affect its function. Second, upstream signaling pathways (such as Nrf2 and CBX8) can regulate GPX4 expression at the transcriptional level, thereby influencing ferroptosis sensitivity [38]. This may explain why in MOLM-13 cells, MAT+RSL3 does not affect GPX4 protein expression levels but can still modulate ferroptosis activity through other mechanisms. Future studies should further explore the post-translational modification mechanisms of GPX4 and its role in ferroptosis, providing new therapeutic targets for related diseases. While the partial induction of ferroptosis in p53 knockdown cells may involve compensatory mechanisms, such as NRF2-mediated upregulation of antioxidant genes, non-coding RNA modulation of ferroptosis sensitivity, or autophagy-dependent pathways like ferritinophagy. These mechanisms underscore the complexity of ferroptosis regulation and warrant further investigation to elucidate alternative pathways driving ferroptosis in the absence of p53. The validated targets, such as p53 and GPX4, are crucial components of the ferroptosis pathway, and our findings suggest that MAT can modulate this pathway to induce cell death. We acknowledge the importance of validating all identified targets and plan to pursue this in future work. Additionally, we plan to conduct detailed immunophenotyping and cytokine profiling studies in both *in vitro* and *in vivo* models. Understanding these immunomodulatory effects could pave the way for combining MAT with immunotherapy strategies (such as checkpoint inhibitors), to achieve even better therapeutic outcomes in AML.

Meanwhile, the combination of MAT and RSL3 significantly reduces p53 protein expression, which may be mediated through post-translational modifications. Upstream regulators such as MDM2 (a key E3 ubiquitin ligase responsible for p53 degradation) or ATM (activated by DNA damage to stabilize p53) could be involved in this process. Further investigation is needed to elucidate the specific roles of these upstream regulators.

We preliminarily evaluated the toxicity of ferroptosis induction in non-leukemic cells using the HS-5. The results showed that the cytotoxic effect of RSL3 on HS-5 cells is much lower compared to its effect on MOLM-13 and MV4-11 cells. Additionally, we found that MAT (1 mM) did not enhance the inhibitory effect of RSL3 on HS-5 cell proliferation, suggesting that the combination of MAT and RSL3 has a favorable safety profile. This may be because the differential expression of key targets such as p53, RELA, CASP3, MYC, PTEN, and CCND1 between AML and healthy samples plays a crucial role in defining the therapeutic window of MAT. AML cells, with their altered expression profiles, exhibit heightened sensitivity to MAT-induced ferroptosis, while healthy cells remain relatively unaffected. This selectivity enhances the potential safety and efficacy of MAT as a therapeutic agent for AML. In future studies, we plan to further evaluate the safety of ferroptosis induction using human bone marrow samples and animal models to provide a more comprehensive assessment.

Moreover, the results presented in this study, while promising and indicating potential therapeutic avenues for further exploration, are derived from cell lines and a mouse model. While such preclinical models are essential for initial validation of scientific hypotheses and therapeutic strategies, it is important to note the limitations associated with their translation to human disease. Specifically, the lack of human tissue data or patient-derived xenografts represents a significant gap that needs to be addressed in future studies. Meanwhile, the future perspective that the long-term adverse effects of MAT and RSL3 combination therapy warrants further evaluation to provide critical insights into the therapeutic window and potential risks associated with MAT and RSL3 treatment. In future research, we plan to incorporate long-term experiments in our animal models to monitor the development of sec-

ondary malignancies and other potential delayed adverse effects. These investigations will provide a more comprehensive understanding of the safety profile of MAT + RSL3 combination therapy and its implications for clinical application. Our current p53 knockdown experiments have demonstrated that MAT enhances RSL3-induced ferroptosis via the p53 signaling pathway. Future studies will require p53 overexpression to validate the causal relationship between p53 activation and ferroptosis induction.

Given the heterogeneity within MLL-r AML, we acknowledge that findings from these two cell lines may not be directly generalizable to all MLL-r AML subtypes. Nonetheless, our results provide important insights into the biological mechanisms and potential therapeutic vulnerabilities shared by at least some MLL-r AML subtypes. To enhance the generalizability of our findings, we plan to extend our studies to additional MLL-r AML cell lines and primary patient samples in future work. Since our preclinical outcomes cannot encompass all MLL-rearranged AML patients, their clinical translation must be approached with caution, emphasizing personalized medicine to identify patients most likely to benefit from RSL3- and MAT-based therapies.

In the context of AML therapy, resistance to treatment is a significant challenge. To address potential resistance mechanisms that may arise with MAT + RSL3 therapy, we propose investigating the molecular basis of resistance, such as genetic mutations or altered metabolic pathways, and exploring combination strategies with targeted therapies or resistance pathway inhibitors. Future studies employing transcriptomic and proteomic approaches will be required to comprehensively elucidate the molecular pathways involved and to further strengthen the mechanistic basis of MAT-mediated ferroptosis sensitization in MLL-r AML. Additionally, synthetic optimization of MAT to enhance its efficacy and specificity may further mitigate resistance. These approaches will be validated through preclinical and clinical studies to ensure their effectiveness in overcoming resistance in AML therapy. Based on the current research landscape, the optimization of MAT through structural modifications, targeting ferroptosis pathways, and leveraging computational techniques holds promise for enhancing its ferroptosis-inducing capabilities and specificity for AML cells. For instance, integrating anti-tumor active molecular fragments into the MAT structure has been a successful strategy in other cancer therapies. This approach has been used to enhance the potency of MAT2A inhibitors, which target the methionine metabolism pathway [39]. Similarly, targeting key ferroptosis regulators, such as ACSL4 and GPX4, has been shown to induce ferroptosis in various cancer types [40]. Additionally, AI-driven drug design has been employed to generate more potent and selective derivatives of other anticancer agents, which could potentially be applied to MAT optimization [41]. Future work may focus on combining these strategies to develop MAT derivatives with enhanced ferroptosis-inducing capabilities and specificity for AML cells.

Conclusion

In summary, combining MAT with a non-toxic dose of RSL3 to induce ferroptosis synergistically enhanced cell death, possibly via the p53/SLC7A11/GPX4 pathway regulation. Additional research is required to evaluate the clinical applicability of this strategy.

Acknowledgements

We thank Dr. Ya-Huei Kuo from City of Hope Medical Center (Duarte, CA 91010, USA) for her intellectual advice and systematically training to Dr. Dijiong Wu during 1th Oct 2017 to 28th Feb 2019. The present study was supported by the Joint TCM Science & Technology Projects of National Demonstration Zones for Comprehensive TCM Reform (No. GZY-KJS-ZJ-2026-006), Zhejiang Provincial Natural Science Foundation (No. LY21H290003), National Natural Science Foundation of China (No. 81503296), Zhejiang Scientific Research Fund of Traditional Chinese Medicine (No. 2020ZB085), Specific Program of Scientific Research of Zhejiang Chinese Medicine University for Affiliated Hospital (No. 2023FSYY-ZZ04), Project of Academic Inheritance Studio of Famous and Aged Chinese Medicine Experts in Zhejiang Province (No. GZS2021022) and 2024 Zhejiang Chinese Medicine University Postgraduate Scientific Research Fund Project (No. 2024YKJ01).

Disclosure of conflict of interest

None.

Address correspondence to: Drs. Dijiong Wu and Keding Shao, Department of Hematology, The First Affiliated Hospital of Zhejiang Chinese Medical University, Hangzhou 310005, Zhejiang, P. R. China. Tel: +86-0571-86620325; E-mail: wudijiong@zcmu.edu.cn (DJW); Tel: +86-13858175956; E-mail: skd@zcmu.edu.cn (KDS)

References

[1] Stavropoulou V, Kaspar S, Brault L, Sanders MA, Juge S, Morettini S, Tzankov A, Iacovino M, Lau IJ, Milne TA, Royo H, Kyba M, Valk PJM, Peters AHFM and Schwaller J. MLL-AF9 expression in hematopoietic stem cells drives a highly invasive AML expressing EMT-related genes linked to poor outcome. Cancer Cell 2016; 30: 43-58.

[2] El Chaer F, Keng M and Ballen KK. MLL-rearranged acute lymphoblastic leukemia. Curr Hematol Malig Rep 2020; 15: 83-89.

[3] Meyer C, Hofmann J, Burmeister T, Gröger D, Park TS, Emerenciano M, Pombo de Oliveira M, Renneville A, Villarese P, Macintyre E, Cavé H, Clappier E, Mass-Malo K, Zuna J, Trka J, De Braekeleer E, De Braekeleer M, Oh SH, Tsaur G, Fechina L, van der Velden VH, van Dongen JJ, Delabesse E, Binato R, Silva ML, Kustanovich A, Aleinikova O, Harris MH, Lund-Aho T, Juvonen V, Heidenreich O, Vormoor J, Choi WW, Jarosova M, Kolenova A, Bueno C, Menendez P, Wehner S, Eckert C, Talmant P, Tondeur S, Lippert E, Launay E, Henry C, Ballerini P, Lapillone H, Callanan MB, Cayuela JM, Herbaux C, Cazzaniga G, Kakadiya PM, Bohlander S, Ahlmann M, Choi JR, Gameiro P, Lee DS, Krauter J, Cornillet-Lefebvre P, Te Kronnie G, Schäfer BW, Kubetzko S, Alonso CN, zur Stadt U, Sutton R, Venn NC, Izraeli S, Trakhtenbrot L, Madsen HO, Archer P, Hancock J, Cerveira N, Teixeira MR, Lo Nigro L, Möricke A, Stanulla M, Schrappe M, Sedék L, Szczepański T, Zwaan CM, Coenen EA, van den Heuvel-Eibrink MM, Strehl S, Dworzak M, Panzer-Grümayer R, Dingermann T, Klingebiel T and Marschalek R. The MLL recombinome of acute leukemias in 2013. Leukemia 2013; 27: 2165-2176.

[4] Chan AKN and Chen CW. Rewiring the epigenetic networks in MLL-rearranged leukemias: epigenetic dysregulation and pharmacological interventions. Front Cell Dev Biol 2019; 7: 81.

[5] Olsen SN, Godfrey L, Healy JP, Choi YA, Kai Y, Hatton C, Perner F, Haarer EL, Nabet B, Yuan GC and Armstrong SA. MLL::AF9 degradation induces rapid changes in transcriptional elongation and subsequent loss of an active chromatin landscape. Mol Cell 2022; 82: 1140-1155, e11.

[6] Dong LH, Huang JJ, Zu P, Liu J, Gao X, Du JW and Li YF. CircKDM4C upregulates P53 by sponging hsa-let-7b-5p to induce ferroptosis in acute myeloid leukemia. Environ Toxicol 2021; 36: 1288-1302.

[7] Stockwell BR, Jiang X and Gu W. Emerging mechanisms and disease relevance of ferroptosis. Trends Cell Biol 2020; 30: 478-490.

[8] Feng S, Yuan Y, Lin Z, Li M, Ye D, Shi L, Li D, Zhao M, Meng C, He X, Wu S, Xiong F, Ye S, Yang J, Zhuang H, Hong L and Gao S. Low-dose hypomethylating agents cooperate with ferroptosis inducers to enhance ferroptosis by regulating the DNA methylation-mediated MAGEA6-AMPK-SLC7A11-GPX4 signaling pathway in acute myeloid leukemia. Exp Hematol Oncol 2024; 13: 19.

[9] Hassannia B, Vandenabeele P and Vanden Berghe T. Targeting ferroptosis to iron out cancer. Cancer Cell 2019; 35: 830-849.

[10] Yang C, Mi X, Su H, Yang J, Gu Y, Zhang L, Sun W, Liang X and Zhang C. GE11-PDA-Pt@USPIOs nano-formulation for relief of tumor hypoxia and MRI/PAI-guided tumor radio-chemotherapy. Biomater Sci 2019; 7: 2076-2090.

[11] Sun XY, Jia LY, Rong Z, Zhou X, Cao LQ, Li AH, Guo M, Jin J, Wang YD, Huang L, Li YH, He ZJ, Li L, Ma RK, Lv YF, Shao KK, Zhang J and Cao HL. Research advances on Matrine. Front Chem 2022; 10: 867318.

[12] Hao Y, Ji J, Liu C, Zhang N and Gong Y. Effects of matrine combined with LY294002 on proliferation, apoptosis and cell cycle of human myeloid leukemia K562 cells. Nan Fang Yi Ke Da Xue Xue Bao 2022; 42: 1739-1746.

[13] Wu DJ, Zhou YH, Zhu J, Zhao W, Zhong WJ, Wang Z, Qian H, Li R, Fu S and Sun J. Study on matrine alleviating retinoic acid resistance in acute promyelocytic leukemia. Zhonghua Xue Ye Xue Za Zhi 2011; 32: 313-316.

[14] Jin J, Fan Z, Long Y, Li Y, He Q, Yang Y, Zhong W, Lin D, Lian D, Wang X, Xiao J and Chen Y. Matrine induces ferroptosis in cervical cancer through activation of piezo1 channel. Phytomedicine 2024; 122: 155165.

[15] Gu J, Zhang Y, Wang X, Xiang J, Deng S, Wu D, Chen J, Yu L, Zhou Y, Wang Y and Shen J. Matrine inhibits the growth of natural killer/T-cell lymphoma cells by modulating CaMKIIgamma-c-Myc signaling pathway. BMC Complement Med Ther 2020; 20: 214.

[16] Wu D, Shao K, Sun J, Zhu F, Ye B, Liu T, Shen Y, Huang H and Zhou Y. Matrine cooperates with all-trans retinoic acid on differentiation induction of all-trans retinoic acid-resistant acute

promyelocytic leukemia cells (NB4-LR1): possible mechanisms. Planta Med 2014; 80: 399-408.
[17] Wu D, Shao K, Zhou Q, Sun J, Wang Z, Yan F, Liu T, Wu X, Ye B, Huang H and Zhou Y. Autophagy and ubiquitin-mediated proteolytic degradation of PML/Raralpha fusion protein in matrine-induced differentiation sensitivity recovery of ATRA-resistant APL (NB4-LR1) cells: in vitro and in vivo studies. Cell Physiol Biochem 2018; 48: 2286-2301.
[18] Wu D, Li M, Hong Y, Jin L, Liu Q, Sun C, Li L, Han X, Deng S, Feng Y, Shen Y and Kai G. Integrated stress response activation induced by usnic acid alleviates BCL-2 inhibitor ABT-199 resistance in acute myeloid leukemia. J Adv Res 2025; 74: 621-635.
[19] Zhang Y, Wu Q, Yuan B, Huang Y, Jiang L, Liu F, Yan P, Jiang Y, Ye J and Jiang X. Influence on therapeutic outcome of platelet count at diagnosis in patients with de novo non-APL acute myeloid leukemia. BMC Cancer 2023; 23: 1030.
[20] Yan HF, Zou T, Tuo QZ, Xu S, Li H, Belaidi AA and Lei P. Ferroptosis: mechanisms and links with diseases. Signal Transduct Target Ther 2021; 6: 49.
[21] Chen X, Kang R, Kroemer G and Tang D. Broadening horizons: the role of ferroptosis in cancer. Nat Rev Clin Oncol 2021; 18: 280-296.
[22] Ma Z, Ye W, Huang X, Li X, Li F, Lin X, Hu C, Wang J, Jin J, Zhu B and Huang J. The ferroptosis landscape in acute myeloid leukemia. Aging (Albany NY) 2023; 15: 13486-13503.
[23] Tang X, Wang Y, Zhu Y, Guo Y and Liu B. Basic mechanisms and novel potential therapeutic targets for ferroptosis in acute myeloid leukemia. Ann Hematol 2023; 102: 1985-1999.
[24] Stockwell BR, Friedmann Angeli JP, Bayir H, Bush AI, Conrad M, Dixon SJ, Fulda S, Gascón S, Hatzios SK, Kagan VE, Noel K, Jiang X, Linkermann A, Murphy ME, Overholtzer M, Oyagi A, Pagnussat GC, Park J, Ran Q, Rosenfeld CS, Salnikow K, Tang D, Torti FM, Torti SV, Toyokuni S, Woerpel KA and Zhang DD. Ferroptosis: a regulated cell death nexus linking metabolism, redox biology, and disease. Cell 2017; 171: 273-285.
[25] Huang J and Xu H. Matrine: bioactivities and structural modifications. Curr Top Med Chem 2016; 16: 3365-3378.
[26] Gao Y, Wu C, Huang J, Huang Z, Jin Z, Guo S, Tao X, Lu S, Zhang J, Zhang F, Zhai Y, Shi R, Ye P and Wu J. A new strategy to identify ADAM12 and PDGFRB as a novel prognostic biomarker for matrine regulates gastric cancer via high throughput chip mining and computational verification. Comput Biol Med 2023; 166: 107562.
[27] Lei G, Zhuang L and Gan B. Targeting ferroptosis as a vulnerability in cancer. Nat Rev Cancer 2022; 22: 381-396.
[28] Lei G, Mao C, Yan Y, Zhuang L and Gan B. Ferroptosis, radiotherapy, and combination therapeutic strategies. Protein Cell 2021; 12: 836-857.
[29] Ursini F and Maiorino M. Lipid peroxidation and ferroptosis: the role of GSH and GPx4. Free Radic Biol Med 2020; 152: 175-185.
[30] Battaglia AM, Chirillo R, Aversa I, Sacco A, Costanzo F and Biamonte F. Ferroptosis and cancer: mitochondria meet the "iron maiden" cell death. Cells 2020; 9: 1505.
[31] Liao XM, Chen Q, Feng ZX, Yang XM and Zhu CY. Construction and identification of acute myeloid leukemia NOD/SCID mouse model by tail vein injection of THP-1 cells. Zhongguo Shi Yan Xue Ye Xue Za Zhi 2020; 28: 424-429.
[32] Wang D, Kaniowski D, Jacek K, Su YL, Yu C, Hall J, Li H, Feng M, Hui S, Kaminska B, DeFranciscis V, Esposito CL, DiRuscio A, Zhang B, Marcucci G, Kuo YH and Kortylewski M. Bifunctional CpG-STAT3 decoy oligonucleotide triggers multilineage differentiation of acute myeloid leukemia in mice. Mol Ther Nucleic Acids 2024; 35: 102268.
[33] Liu J, Zhou HY, Xu T and Liu XD. Prediction of potential drug activity and therapeutic targets of a natural compound Niga-ichigoside F1 based on network pharmacology and molecular docking. World Journal of Integrated Traditional and Western Medicine 2023; 9: 40-48.
[34] Long J, Jia MY, Fang WY, Chen XJ, Mu LL, Wang ZY, Shen Y, Xiang RF, Wang LN, Wang L, Jiang CH, Jiang JL, Zhang WJ, Sun YD, Chang L, Gao WH, Wang Y, Li JM, Hong DL, Liang AB and Hu J. FLT3 inhibition upregulates HDAC8 via FOXO to inactivate p53 and promote maintenance of FLT3-ITD+ acute myeloid leukemia. Blood 2020; 135: 1472-1483.
[35] Cai Y, Lv L, Lu T, Ding M, Yu Z, Chen X, Zhou X and Wang X. alpha-KG inhibits tumor growth of diffuse large B-cell lymphoma by inducing ROS and TP53-mediated ferroptosis. Cell Death Discov 2023; 9: 182.
[36] Wang H, Guo M, Wei H and Chen Y. Targeting p53 pathways: mechanisms, structures, and advances in therapy. Signal Transduct Target Ther 2023; 8: 92.
[37] Chu B, Kon N, Chen D, Li T, Liu T, Jiang L, Song S, Tavana O and Gu W. ALOX12 is required for p53-mediated tumour suppression through a distinct ferroptosis pathway. Nat Cell Biol 2019; 21: 579-591.
[38] Yang WS, SriRamaratnam R, Welsch ME, Shimada K, Skouta R, Viswanathan VS, Cheah

JH, Clemons PA, Shamji AF, Clish CB, Brown LM, Girotti AW, Cornish VW, Schreiber SL and Stockwell BR. Regulation of ferroptotic cancer cell death by GPX4. Cell 2014; 156: 317-331.

[39] Guo J, Yang Y, Buettner R and Rosen ST. Targeting the methionine-methionine adenosyl transferase 2A- S -adenosyl methionine axis for cancer therapy. Curr Opin Oncol 2022; 34: 546-551.

[40] Dai E, Chen X, Linkermann A, Jiang X, Kang R, Kagan VE, Bayir H, Yang WS, Garcia-Saez AJ, Ioannou MS, Janowitz T, Ran Q, Gu W, Gan B, Krysko DV, Zhu X, Wang J, Krautwald S, Toyokuni S, Xie Y, Greten FR, Yi Q, Schick J, Liu J, Gabrilovich DI, Liu J, Zeh HJ, Zhang DD, Yang M, Iovanna J, Kopf M, Adolph TE, Chi JT, Li C, Ichijo H, Karin M, Sankaran VG, Zou W, Galluzzi L, Bush AI, Li B, Melino G, Baehrecke EH, Lotze MT, Klionsky DJ, Stockwell BR, Kroemer G and Tang D. A guideline on the molecular ecosystem regulating ferroptosis. Nat Cell Biol 2024; 26: 1447-1457.

[41] Li J, Wei S, Marabada D, Wang Z and Huang Q. Research progress of natural matrine compounds and synthetic matrine derivatives. Molecules 2023; 28: 5780.

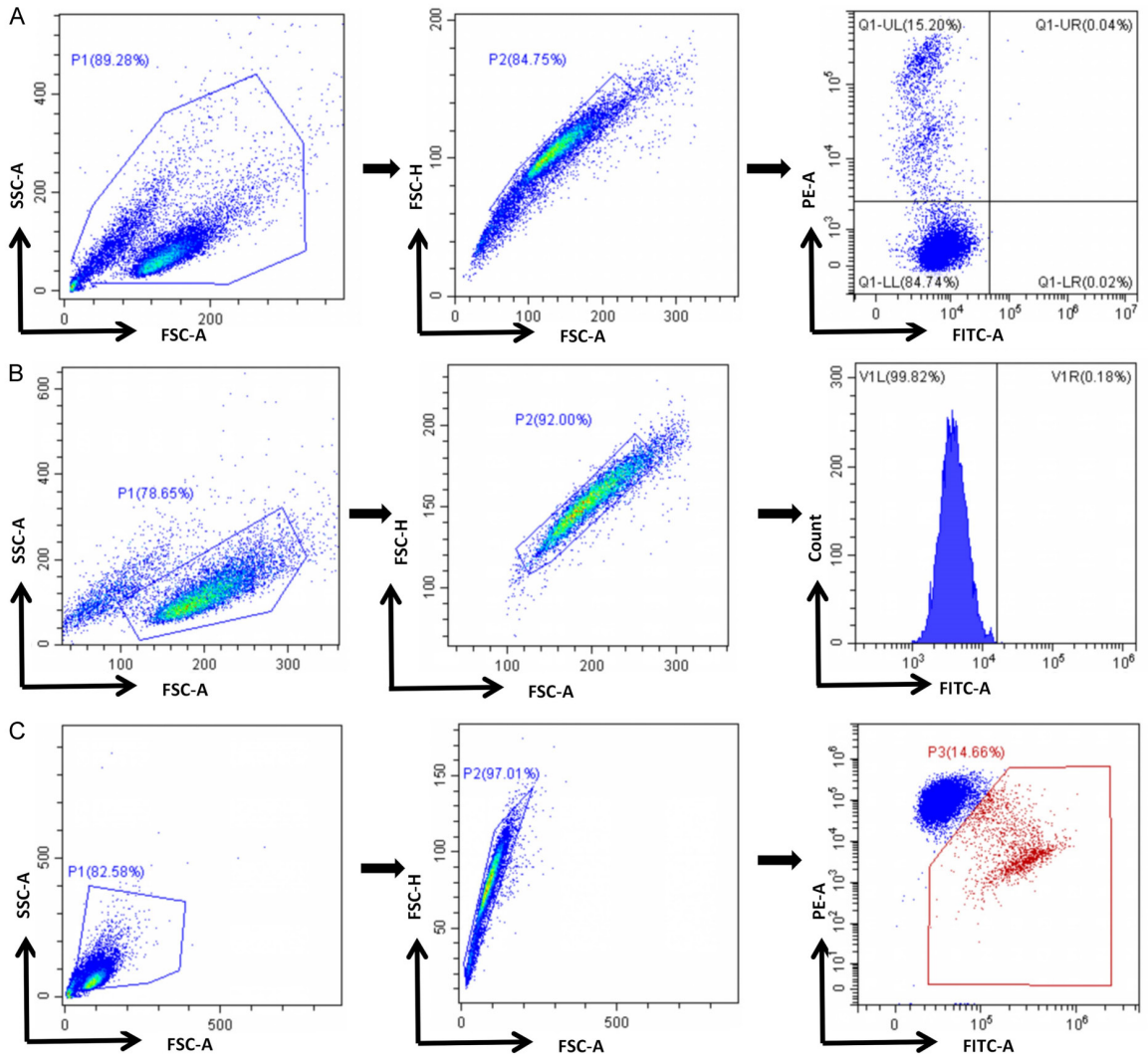

Supplementary Figure 1. Representative Fluorescence-Activated Cell Sorting (FACS) plots showing gating strategy and frequency of (A) Apoptosis/necrosis, (B) Lipid peroxidation and (C) Mitochondrial membrane potential.

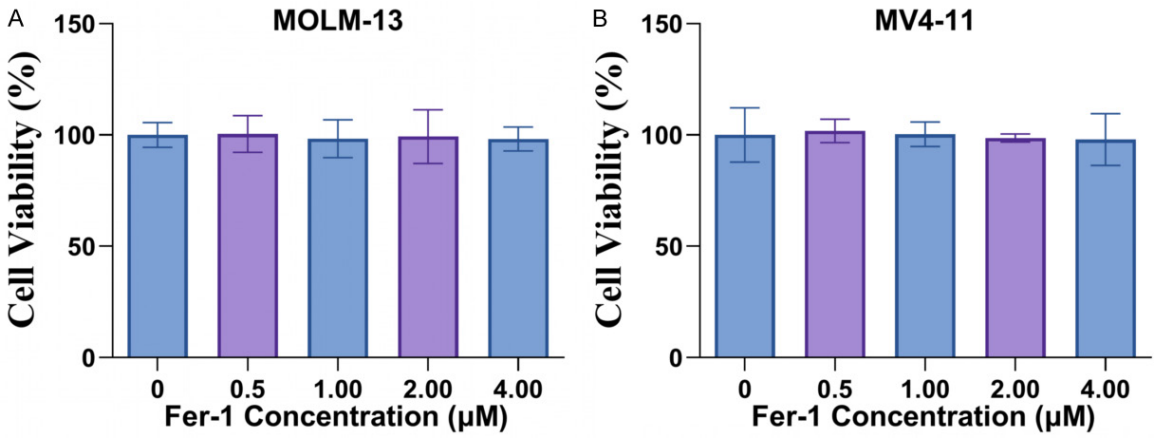

Supplementary Figure 2. Analysis of the effect of different concentrations of Fer-1 on cell viability. Different concentrations of Fer-1 were used to act on (A) MOLM-13 and (B) MV4-11 cell lines for different durations.

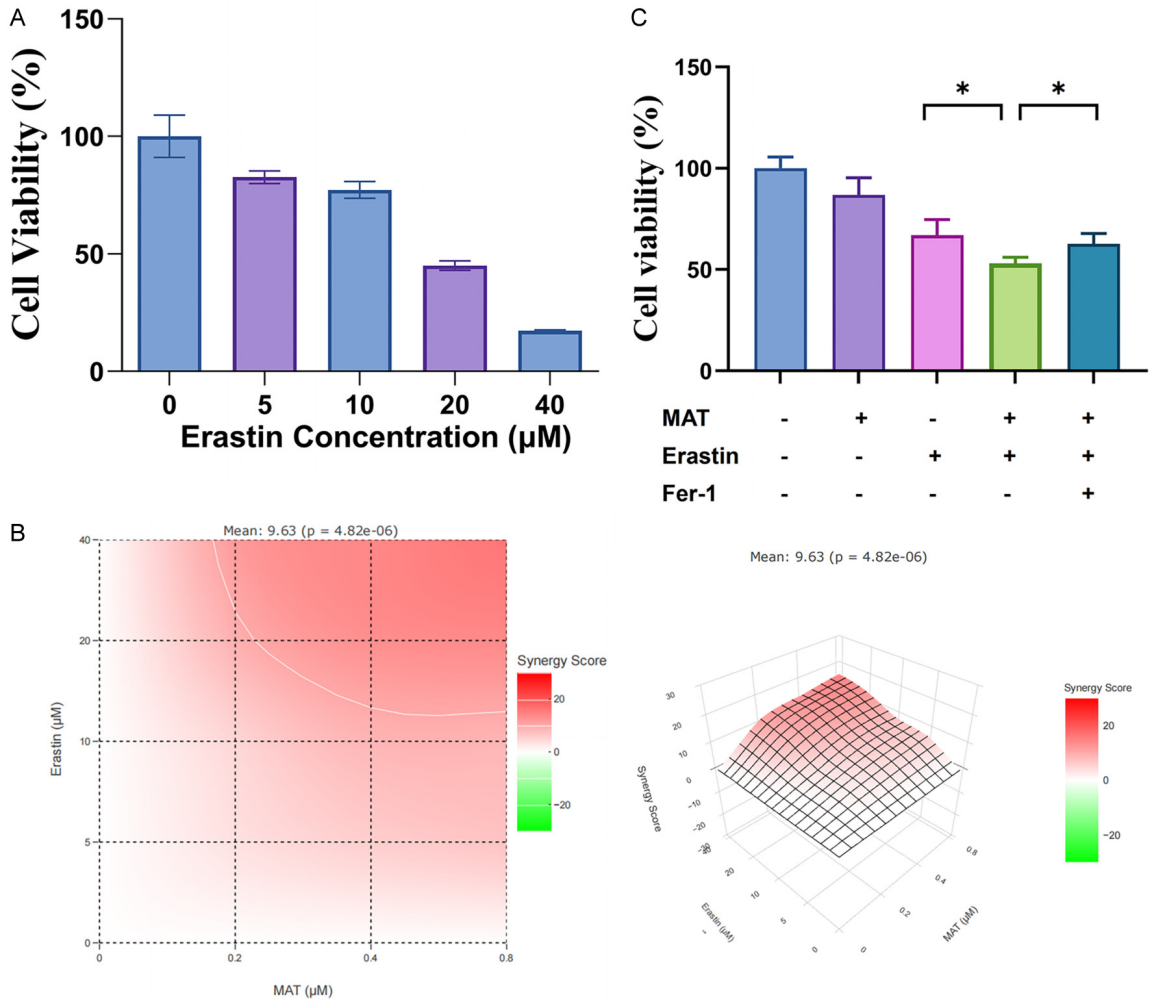

Supplementary Figure 3. The effect of matrine (MAT) combined with the ferroptosis inducer Erastin on MLL-r cell. A. Different concentrations of Erastin were used to act on MOLM-13 for different durations. B. Synergy score of MAT combined with Erastin in the treatment of MOLM-13. C. The ferroptosis inhibitor Fer-1 incompletely reverses the cell death caused by matrine combined with Erastin.

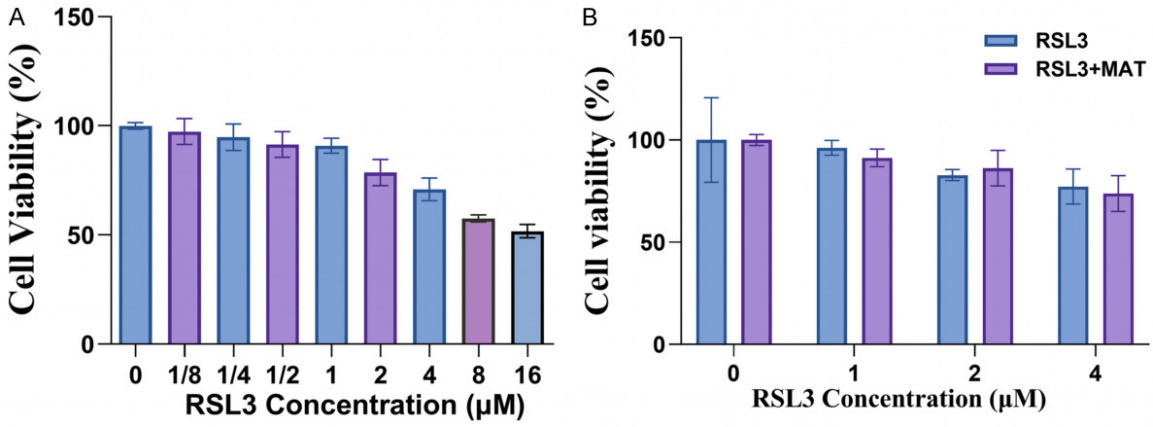

Supplementary Figure 4. The effect of MAT combined with the RSL3 on marrow stroma cell HS-5. A. Different concentrations of Erastin were used to act on HS-5 for different durations. B. MAT combined with different concentrations of RSL3 acted on HS-5 cells.

Supplemental Table1. Analysis of blood routine indexes in MOLM-13 xenograft NSG mice

Test items	Vehicle	MAT	RSL3	Combo	Ara-c+DNR
WBC (10^9/L)	3.56±1.82	4.11±1.39	3.23±1.39	2.27±1.11	3.17±1.21
Gran# (10^9/L)	1.17±0.82	1.05±0.82	1.24±0.84	1.02±0.28	0.9±0.42
Lym# (10^9/L)	1.22±0.52	1.46±0.67	0.95±0.74	0.85±0.46	1.1±0.5
Mon# (10^9/L)	1.16±0.87	1.59±0.74	1.03±0.8	1.29±0.51	1.16±0.55
RBC (10^{12}/L)	7.99±0.69	9.48±0.95	8.99±2.01	7.67±2.04	9.05±1.08
HGB (g/L)	142.83±10.75	163.14±11.83	153.85±29.11	134.14±36.47	159±21.09
HCT (%)	37.93±2.88	44.84±4.22	43.22±9.45	36.87±9.61	43.67±5.15
MCV (fL)	47.46±1.02	47.3±0.61	48.11±0.38	48.12±0.71	48.25±0.81
MCH (pg)	17.91±0.43	17.22±0.48	17.24±0.97	17.37±0.63	17.54±0.57
MCHC (g/L)	377.16±8.18	364.28±9.99	358.14±18.82	361±12.71	363.57±17.37
RDW-CV (%)	13.21±0.72	13.3±0.6	13.3±0.28	13.25±0.33	13.4±0.72
RDW-SD (fL)	24.3±1.85	24.37±1.21	24.77±0.43	24.74±0.64	25.04±1.47
PLT (10^9/L)	296.5±102.61	442.14±151.82	354±136.93	332.42±179.11	649.14±354.73*
MPV (fL)	6.61±0.32	6.97±0.42	7.15±0.21	7.02±0.62	6.3±0.43
PDW (%)	15.66±0.43	15.61±0.29	15.82±0.25	15.91±0.36	15.3±0.31
PCT (%)	0.19±0.06	0.3±0.09	0.25±0.09	0.23±0.12	0.39±0.19
P-LCC (10^9/L)	132.33±40.81	216±62.01	178.28±68.18	169.71±92.03	249.28±103.13
P-LCR (%)	45.36±4.1	49.61±4.75	50.3±4.01	49.07±7.85	40.38±5.77

Note: NSG, Severe immunodeficient mice; Ara-c, Cytarabine; DNR, Daunorubicin; WBC, White Blood Cell count; Gran#, Granulocyte count; Lym#, Lymphocyte count; Mon#, Monocyte count; RBC, Red Blood Cell count; HGB, Hemoglobin; HCT, Hematocrit; MCV, Mean Corpuscular Volume; MCH, Mean Corpuscular Hemoglobin; MCHC, Mean Corpuscular Hemoglobin Concentration; RDW-CV, Red Cell Distribution Width - Coefficient of Variation; RDW-SD, Red Cell Distribution Width - Standard Deviation; PLT, Platelet count; MPV, Mean Platelet Volume; PDW, Platelet Distribution Width; PCT, Plateletcrit; P-LCC, Platelet Large Cell Count; P-LCR, Platelet Large Cell Ratio. *P < 0.05, compared with Vehicle group. Values are means ± SD, n = 7. Blood samples were obtained during sacrifice for routine index examination with a blood cell analyzer.